Hindawi Publishing Corporation
Journal of Nanomaterials
Volume 2012, Article ID 393084, 9 pages
doi:10.1155/2012/393084

Research Article

Synthesis and Characterization of $Se_{35}Te_{65-x}Ge_x$ Nanoparticle Films and Their Optical Properties

Numan Salah,[1] Sami S. Habib,[1] Zishan H. Khan,[1] Esam Alarfaj,[2] and Shamshad A. Khan[3]

[1] *Center of Nanotechnology, King Abdulaziz University, Jeddah 21589, Saudi Arabia*
[2] *Department of Physics, Umm Al-Qura University, Makkah 21955, Saudi Arabia*
[3] *Department of Physics, St. Andrew's College, Gorakhpur 273001, India*

Correspondence should be addressed to Numan Salah, alnumany@yahoo.com

Received 24 October 2011; Revised 1 December 2011; Accepted 15 December 2011

Academic Editor: Marinella Striccoli

Thin films of $Se_{35}Te_{65-x}Ge_x$ ($x = 0, 3, 6, 9, 12$) nanoparticles were synthesized using thermal evaporation method. They were characterized by X-ray diffraction (XRD), scanning electron microscope (SEM), and absorption and transmission spectra. XRD results show that these films are of amorphous nature, while SEM images show nanoparticles with average particle size around 30 nm. No significant changes are observed in morphology of the deposited films by changing concentrations of Te and Ge. The optical behaviors of these films have been studied using the absorption and transmission spectra in the spectral region 400–1100 nm. The absorption, extinction coefficients and refractive index were obtained and investigated in more detail. The optical band gap (E_g) values were also determined and are found to decrease from 0.83 to 0.69 eV by increasing the concentration of Ge from 0 to 12. The transmission spectra for the thin films of $Se_{35}Te_{65-x}Ge_x$ nanoparticles show strong absorption at wavelength less than 500 nm and become highly transparent at wavelength above 800 nm. No significant changes in the transmission spectra are observed by increasing concentration of Ge. These results might be useful for development of optical disks and other semiconducting devices based on these nanochalcogenides.

1. Introduction

In recent years, there has been considerable interest to prepare a variety of nanochalcogenide materials for various applications such as nanomemory devices, nanoelectronic devices, and optical memory devices. The quantum efficiency of chalcogenide materials is high due to the direct band gap. The use of thin film chalcogenides semiconductors has attracted much interest in an expanding variety of applications in various devices. Studies on nanochalcogenides are still at the beginning, and, accordingly, overall features have not been discovered, therefore, there is a lot of scope for the studying these materials in nanometric scale.

Several studies were focused on producing different nanostructures of different amorphous alloys/crystalline materials and study their properties. For example Shi et al. [1] have studied the structural evaluation of mechanically alloyed nanocrystalline FeAl intermetallics, Zakeri et al. [2] have synthesized Bi_2Te_3 nanocrystalline materials by using mechanical alloying, Rafea et al. [3] have studied the structural and optical properties of nanosized $Zn_{0.5}Cd_{0.5}S$ thin films prepared by dip-coating methods, Yang et al. [4] have performed controlled synthesis and characterization of ZnSe nanostructures by using solvothermal approach in a mixed solution, Tripathi et al. [5] have studied the optical properties of Se-Te nanostructured thin films grown by thermal evaporation, and Kotkata et al. [6] have synthesized CdS nanoparticles. The work on temperature and capping dependence of NIR emission from PbS nanomicrocrystallites with different morphologies by Pendyala and Rao [7], synthesis of Ag_2S and Ag_2Se nanoparticles in self-assembled block copolymer micelles and nanoarrays fabrication by Anthony [8], characterization of Bi_2S_3 nanorods and nanostructured flowers prepared by hydrothermal methods by Phuruangrat et al. [9], synthesis of nano-$Cd_xZn_{1-x}S$ by precipitate-hydrothermal methods and their photocatalytic activities by Zu et al. [10],

preparation and properties of nanoamorphous organic and in-organic particles by Senna and Nakayama [11], influence of heat treatment and gamma rays irradiation on the structural and optical characterization of nanocrystalline cobalt phthalocyanine thin films by El-Nahass et al. [12], fabrication of nanocrystalline silicon thin film at low temperature by using a neutral beam deposition method by Kang et al. [13], and analysis of amorphous-nano crystalline multilayer structures by optical, photodeflection, and photocurrent spectroscopy by Gracin et al. [14] are also worth mentioning.

The studies on preparation and characterization of nanocrystalline thin films are also available in the literature by various workers [15–20]. Keeping in view the scope of nanostructure materials, we have communicated several reports [21–24] on synthesis and characterization of nanochalcogenides in both amorphous and crystalline forms by different techniques. Therefore, preparation and characterization of nano-chalcogenide materials are extremely important for application in devices. This work reports on thin films of $Se_{35}Te_{65-x}Ge_x$ ($x = 0, 3, 6, 9, 12$) nanoparticles synthesized using thermal evaporation method. They were characterized by X-ray diffraction (XRD), scanning electron microscope (SEM) and absorption and transmission spectra and investigated in more detail.

2. Experiment

Glassy alloy of $Se_{35}Te_{65-x}Ge_x$ ($x = 0, 3, 6, 9, 12$) is prepared by melt-quenching technique. Materials of 99.999% purity are sealed in quartz ampoules (length 12 cm, internal diameter 0.8 cm) with a vacuum of about 10^{-6} torr. The sealed ampoules are kept inside a furnace where the temperature is raised slowly ($5\,K\cdot min^{-1}$) to 900°C. The ampoules are rocked frequently for 10 h at the maximum temperature to make the melt homogeneous. After rocking, the alloys were quenched in ice water.

Nanoparticles of $Se_{35}Te_{65-x}Ge_x$ were fabricated using physical vapour condensation method. In this method, the starting material is glassy alloys of $Se_{35}Te_{65-x}Ge_x$ in powder form prepared using the above-mentioned technique. Initially, a small quantity of glassy alloy is kept in a molybdenum boat, and the chamber is evacuated to a vacuum of the order of 10^{-6} torr. After reaching this vacuum level, the argon gas is purged inside the chamber. The pressure of the gas is kept constant at 6 torr. The glassy alloy is then evaporated in presence of ambient argon gas atmosphere in the chamber to get the nanostructures. The substrate is cooled with liquid nitrogen, and this evaporated material is deposited on a glass substrate pasted on this cooled substrate. It is worth mentioning here that the nanostructures of glassy alloy are deposited onto cooled substrate, which implies that the material is further quenched at low temperature. This makes the present system completely amorphous. The thickness of the films is measured by using a quartz crystal monitor Edward model FTM 7. The thickness is fixed at 30 nm for all the films. This value was confirmed by measuring thickness of the deposited films using the surface profiler AS 500 Tencor Alpha-Step.

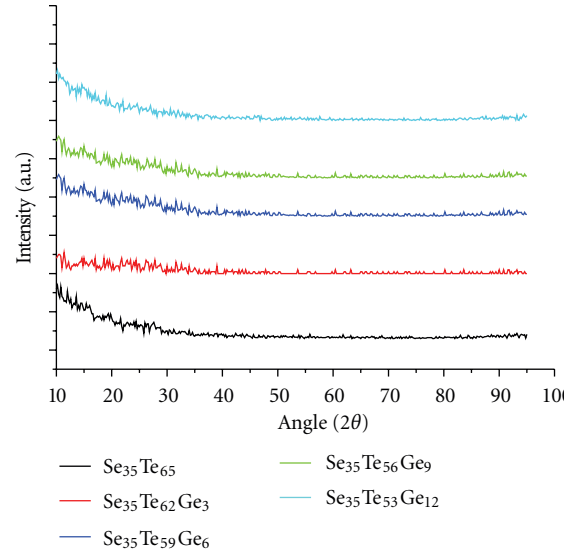

Figure 1: XRD pattern of as-prepared amorphous alloy of $Se_{35}Te_{65-x}Ge_x$ nanoparticle films.

The as-synthesized samples were characterized by X-ray diffraction, using an Ultima-IV (Rigaku, Japan) diffractometer with Cu Kα radiation, while the morphology of these nanostructures is studied by scanning electron microscope (SEM) using Quanta, FEI. The chemical compositions of the deposited films were measured by the energy dispersive spectroscopy (EDS) technique using EDAX, Ametec.

The optical absorption and transmission of thin films of glassy alloy of $Se_{35}Te_{65-x}Ge_x$ ($x = 0, 3, 6, 9, 12$) have been measured by a UV-visible computerized spectrophotometer (model "UV-1650PC", Shimadzu, Japan) in the wavelength region 400–1100 nm. Here, we have kept the samples (films) and reference (glass substrate) in the chamber to neutralize the absorption of glass. The absorption has been measured in terms of optical density. The optical absorption and transmission are measured as a function of incidence photon energy.

3. Results and Discussion

XRD patterns of the as-prepared amorphous alloy of $Se_{35}Te_{65-x}Ge_x$ ($x = 0, 3, 6, 9, 12$) nanoparticles are presented in Figure 1. There are no significant peaks observed for any of the samples. It is clear that the alloys show an amorphous nature. As we mentioned above, the substrate is cooled with liquid nitrogen and the evaporated material is deposited on a glass substrate pasted on this cooled substrate. This implies that the material is further quenched at low temperature, which makes the present system completely amorphous. It is reported that if the substrate temperature is high (~363 K), then the resulting deposited material has a polycrystalline phase [15].

Scanning electron microscopy (SEM) images for the as-synthesized thin films of $Se_{35}Te_{65-x}Ge_x$ nanoparticles are

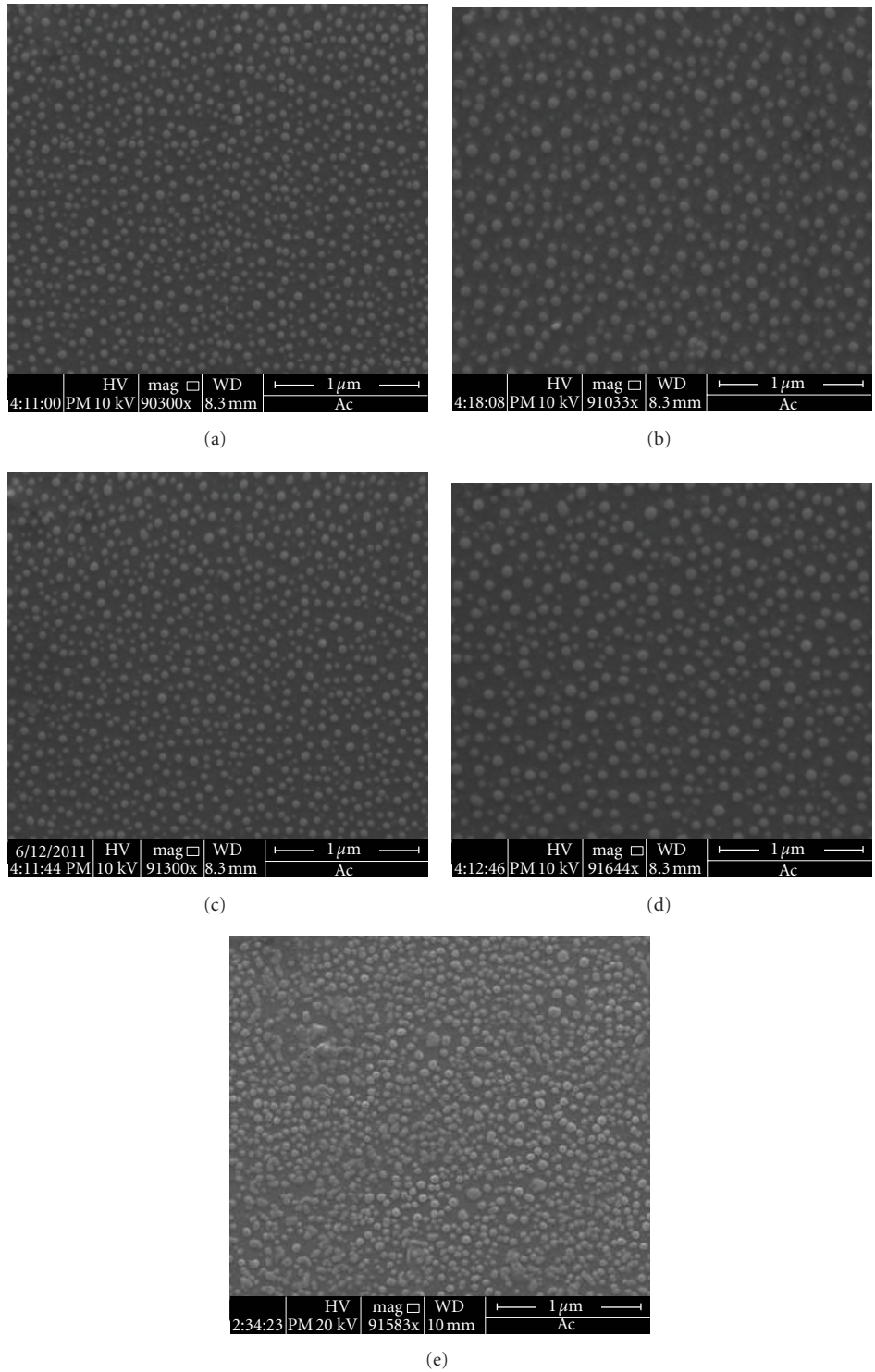

FIGURE 2: SEM images for the as-synthesized thin films of $Se_{35}Te_{65-x}Ge_x$ nanoparticles: (a) $Se_{35}Te_{65}$, (b) $Se_{35}Te_{62}Ge_3$, (c) $Se_{35}Te_{59}Ge_6$, (d) $Se_{35}Te_{56}Ge_9$, and (e) $Se_{35}Te_{53}Ge_{12}$.

obtained and presented in Figures 2(a), 2(b), 2(c), 2(d), and 2(e). This figure shows SEM images of the same magnification for all the samples of $Se_{35}Te_{65-x}Ge_x$ system. Their morphology is almost similar. The average particle size in these films is around 30 nm. The films with high concentration of Ge show shiny nanoparticles, particularly that of $x = 12$. The samples with high values of x seem to be closer to conductors, rather than semiconductor. This will be discussed in the following paragraph after calculating values of the band gaps (E_g). Figure 3 shows typical SEM images of different

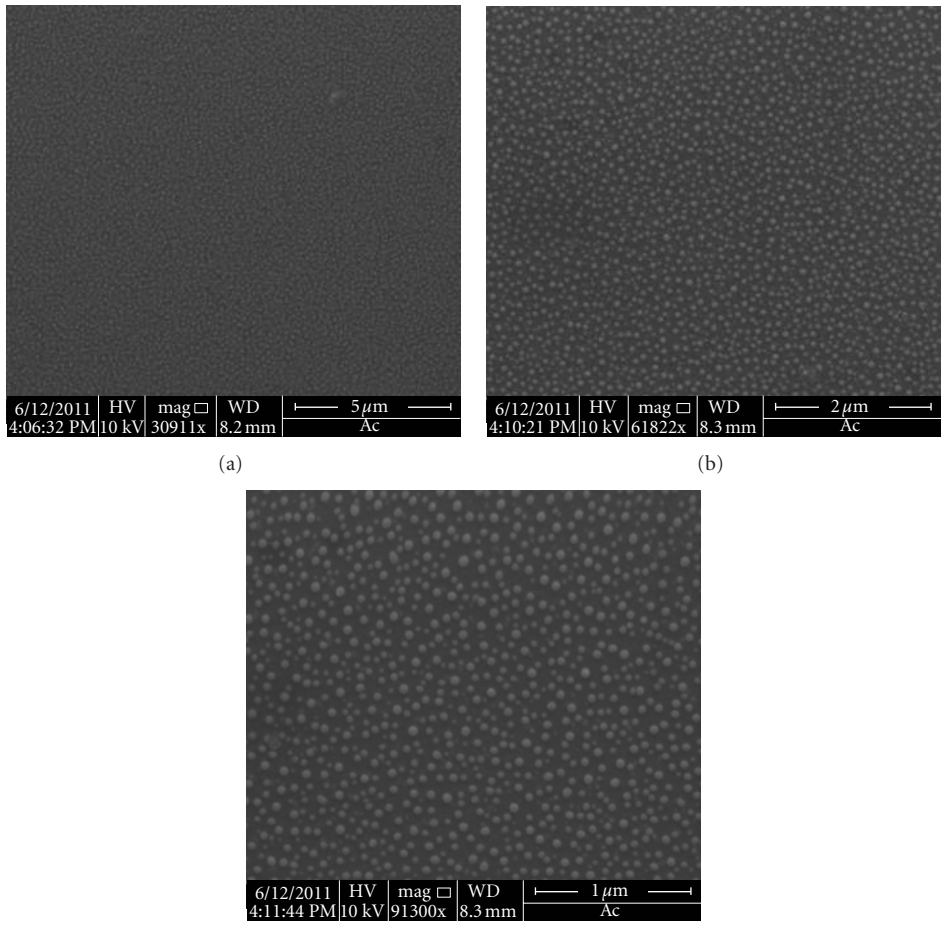

Figure 3: SEM images of different magnifications for the as-synthesized thin films of $Se_{35}Te_{59}Ge_6$ nanoparticles.

magnifications for $Se_{35}Te_{59}Ge_6$. The average size of the grown nanoparticles is around 30 nm. The chemical compositions of the as-grown thin films of $Se_{35}Te_{65-x}Ge_x$ nanoparticles were measured using energy dispersive spectroscopy (EDS) and are presented in Figures 4(a), 4(b), 4(c), 4(d), and 4(e). The EDS results show that the deposited films have compositions close to those of the bulk materials. This figure shows clearly the decrease in Te and increase in Ge concentrations.

Figure 5 shows variation of absorption coefficient (α) with incident photon energy ($h\nu$) for thin films of $Se_{35}Te_{65-x}Ge_x$ nanoparticles. The value of the absorption coefficient has been calculated using the relation

$$\alpha = \frac{\mathrm{OD}}{t}, \tag{1}$$

where OD is the optical density measured at a given layer thickness t.

It is observed that the value of absorption coefficient increases linearly with the increase in photon energy for all the samples of $Se_{35}Te_{65-x}Ge_x$ nanoparticles, while it decreases with increasing Ge concentration. The calculated values for the absorption coefficient at wavelength $\lambda = 800$ nm ($h\nu = 1.54$ eV) are given in Table 1. In the absorption process, a photon of known energy excites an electron from a lower to a higher energy state, corresponding to absorption edge. In chalcogenide glasses, a typical absorption edge can be broadly ascribed to one of the three processes: (i) residual below-gap absorption, (ii) Urbach tails, and (iii) inter-band absorption. Chalcogenide glasses have been found to exhibit highly reproducible optical edges, which are relatively insensitive to preparation conditions, and only the observable absorption [25] with a gap under equilibrium conditions accounts for the first process. In amorphous materials a different type of optical absorption edge is observed and absorption coefficient increases exponentially with the photon energy near the energy gap. These observations are clearly seen in the present $Se_{35}Te_{65-x}Ge_x$ system (Figure 5), and this type of behavior has also been observed in other chalcogenides [26]. This optical absorption edge is known as the Urbach edge and is given by

$$\alpha \sim \frac{\exp[A(h\nu - h\nu_0)]}{KT}, \tag{2}$$

where A is a constant of the order of unity and ν_0 is the constant corresponding to the lowest excitonic frequency. The order of the calculated values of the absorption coefficient

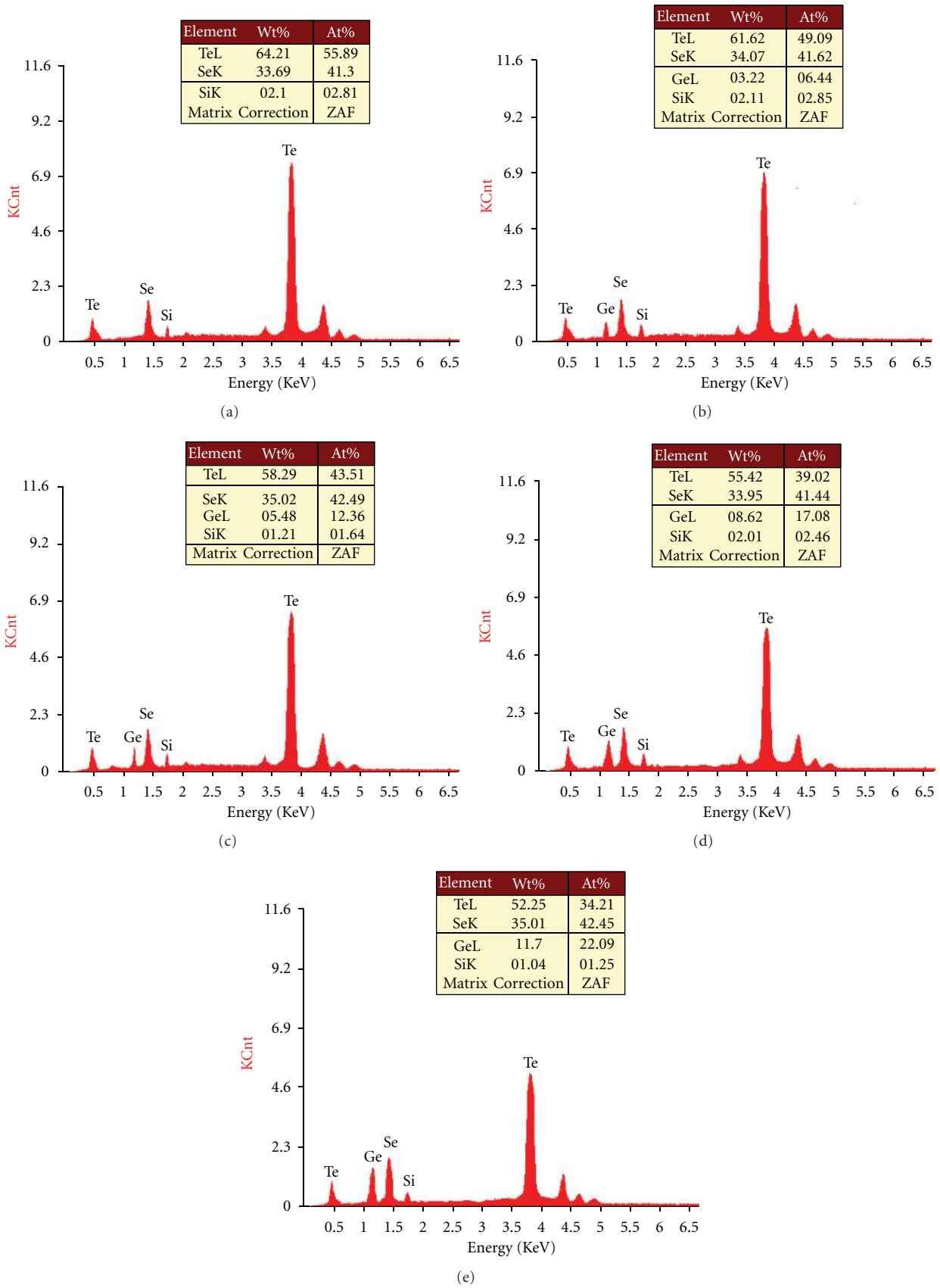

FIGURE 4: EDS quantitative and qualitative results for the as-synthesized thin films of $Se_{35}Te_{65-x}Ge_x$ nanoparticles: (a) $Se_{35}Te_{65}$, (b) $Se_{35}Te_{62}Ge_3$, (c) $Se_{35}Te_{59}Ge_6$, (d) $Se_{35}Te_{56}Ge_9$, and (e) $Se_{35}Te_{53}Ge_{12}$.

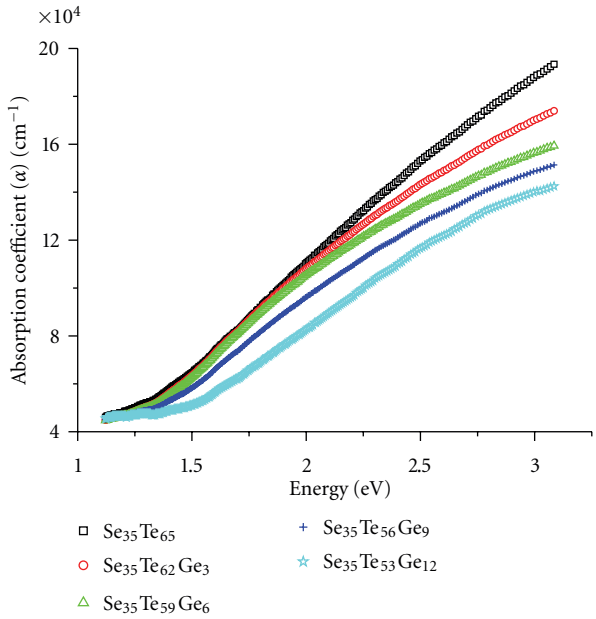

FIGURE 5: Variation of absorption coefficient with incident photon energy ($h\nu$) for thin films of $Se_{35}Te_{65-x}Ge_x$ nanoparticles.

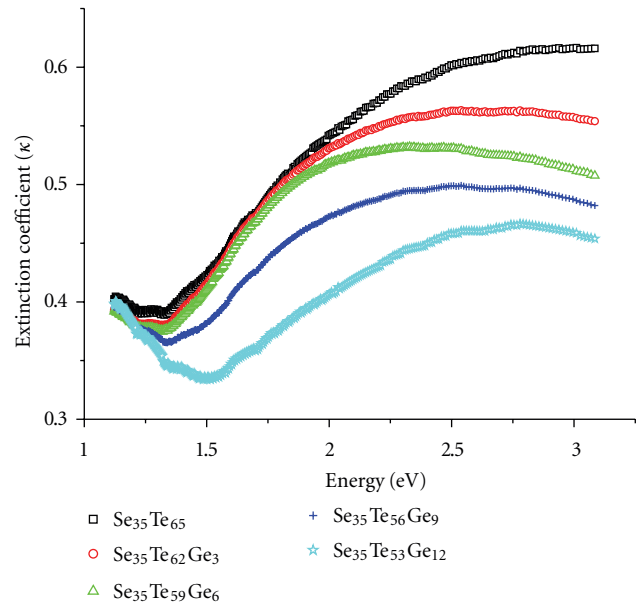

FIGURE 6: Variation of extinction coefficient (k) with incident photon energy ($h\nu$) in thin films of $Se_{35}Te_{65-x}Ge_x$ nanoparticles.

TABLE 1: Optical band gap (E_g), absorption coefficient (α), and extinction coefficient (k) at 800 nm and refractive index (n) for $Se_{35}Te_{65-x}Ge_x$ nanoparticle films.

Sample	E_g (eV)	α (cm^{-1})	k	n
$Se_{35}Te_{65}$	0.83	67670	0.431	2.41
$Se_{35}Te_{62}Ge_3$	0.79	66945.9	0.426	2.53
$Se_{35}Te_{59}Ge_6$	0.75	66415.8	0.423	2.65
$Se_{35}Te_{56}Ge_9$	0.72	61267.4	0.390	2.77
$Se_{35}Te_{53}Ge_{12}$	0.69	53000	0.338	2.86

The uncertainty in E_g is ± 0.01 eV.

for $Se_{35}Te_{65-x}Ge_x$ films is in the range of around 10^4 cm^{-1}, which is consistent with the result of other workers [27].

The optical behavior of materials is important to determine their usage particularly in optoelectronic devices. The value of the extinction coefficient is calculated using the relation

$$k = \frac{\lambda\alpha}{4\pi}. \tag{3}$$

The calculated values of extinction coefficient (k) for $Se_{35}Te_{65-x}Ge_x$ nanoparticles thin films at wavelength λ = 800 nm ($h\nu$ = 1.54 eV) are given in Table 1 and their variation with photon energy is shown in Figure 6. The values of k are observed to decrease at lower photon energy, but beyond 1 eV they exponentially increases. However, these values were significantly decreased by increasing Ge concentration in $Se_{35}Te_{65-x}Ge_x$ nanoparticle films.

The present system of $Se_{35}Te_{65-x}Ge_x$ nanoparticles obeys the rule of indirect transition, and the relation between the optical gap, optical absorption coefficient, and the energy $h\nu$ of the incident photon is given by [3, 16]

$$(\alpha h\nu)^{1/2} \propto \left(h\nu - E_g\right). \tag{4}$$

Figure 7 shows the variation of $(\alpha h\nu)^{1/2}$ with photon energy ($h\nu$) for the thin films of $Se_{35}Te_{65-x}Ge_x$ nanoparticles. The value of indirect optical band gap (E_g) is calculated by taking the intercept on the x-axis. The calculated values of E_g are given in Table 1. It is clear from this table that there is a small change in value of the optical band gap by increasing Ge concentration in this system. The value of E_g at x = 0 is 0.83 eV, while it decreased to 0.69 eV at x = 12. These values are comparable with those of $Ge_{10}Se_{90-x}Te_x$ (x = 0, 10, 20, 30, 40, 50) alloys presented by Sharma and Katyal [15], particularly that of $Ge_{10}Se_{40}Te_{50}$, which has a composition close to some of our samples ($Se_{35}Te_{56}Ge_9$ and $Se_{35}Te_{53}Ge_{12}$). Since the optical absorption depends on short-range order in the amorphous states and defects associated with it, the decrease in optical band gap may be explained on the basis of "density of state model" proposed by Mott and Davis [28]. According to this model, the width of the localized states near the mobility edges depends on the degree of disorder and defects present in the amorphous structure. In particular, it is known that unsaturated bonds together with some saturated bonds are produced as the result of an insufficient number of atoms deposited in the amorphous film [29]. The unsaturated bonds are responsible for the formation of some of the defects in the films, producing localized/defect states in the amorphous solids. In the present system, that is, $Se_{35}Te_{65-x}Ge_x$, the atomic radius of Ge is smaller than that of Te; therefore, it is expected that the number of unsaturated bonds will be increased by increasing concentration of Ge and decreasing that of Te. The presence

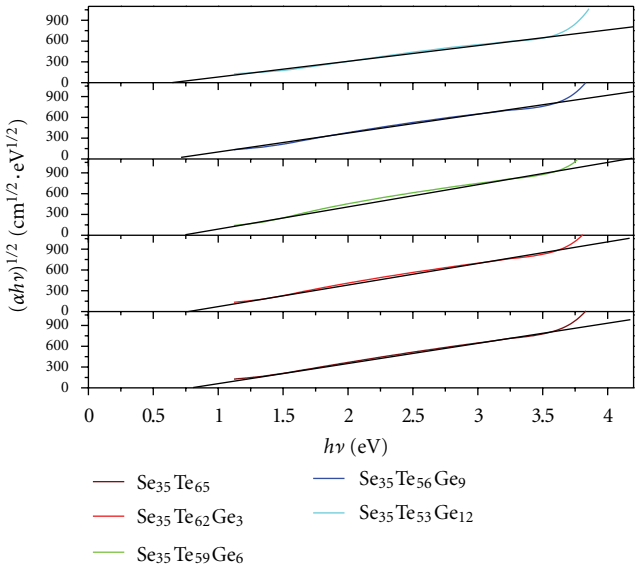

FIGURE 7: $(ahn)^{1/2}$ against photon energy ($h\nu$) for thin films of $Se_{35}Te_{65-x}Ge_x$ nanoparticles.

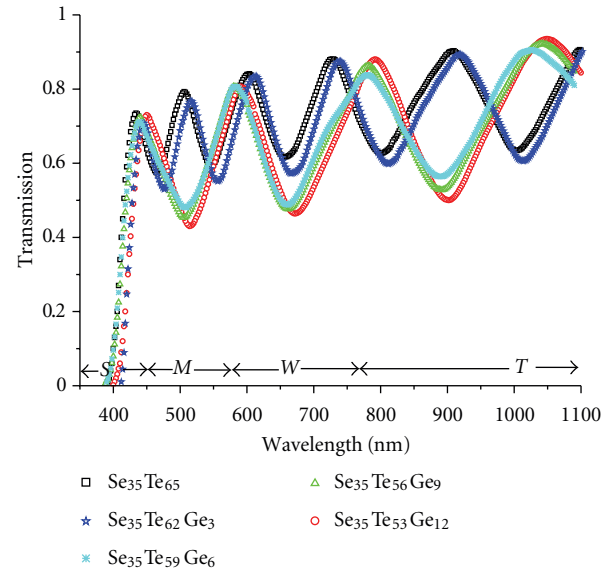

FIGURE 8: Transmission spectra for thin films of $Se_{35}Te_{65-x}Ge_x$ nanoparticles (S: strong absorption, M: medium absorption, W: weak absorption, and T: transparent).

of high concentration of localized/defect states in the band structure is responsible for the decrease in optical band gap on increasing the Ge concentration in these amorphous films of $Se_{35}Te_{65-x}Ge_x$ nanoparticles. This decrease in optical band gap may also be due to the shift in the Fermi level whose position is determined by the distribution of electrons over the localized states [30]. The samples with higher values of x, which are found to have smaller band gap values, become closer to conductors. This might be the reason for a formation of shiny particles by increasing concentration of Ge, particularly that of $x = 12$ ($Se_{35}Te_{53}Ge_{12}$). It is understood that while taking SEM image for insulators or semiconductors, we use to apply a very thin layer of gold on the material to obtain high-resolution images and shiny particles. But for conducting materials, the measurement can be taken directly without a layer of gold. This might be the reason for getting shiny particles in our films that have higher concentrations of Ge.

Figure 8 shows transmission spectra for thin films of $Se_{35}Te_{65-x}Ge_x$ nanoparticles. Optical transmission is a very complex function and strongly depends on absorption coefficient [31]. The spectrum can be divided into four different regions according to their transmission intensities [32]. In the transparent spectral (T) region of the film the value of α is almost ≈ 0, while at the weak absorption (W) the value of α is increased and at medium absorption (M) and strong absorption (S) regions this value is dominating. This variation in the transmission was reported to be determined by the refractive indexes of both the deposited film (n) and that of the substrate (s) [33]. The substrate is several-orders-of-magnitude thicker than the deposited film and has a refractive index $s = 1.51$. If the thickness is uniform, interference effect gives rise to an oscillating spectrum as shown in Figure 8. In the transparent spectral region of the film "$\alpha \approx 0$" the transmission is determined by n and s through multiple reflections. In the transparent region transmission fringe minima T_m can be used to calculate the refractive index of the film which is given by

$$n = \left[M + \left(M^2 - s^2\right)^{1/2}\right]^{1/2}, \tag{5}$$

where

$$M = \frac{2s}{T_m} - \frac{s^2 + 1}{2}. \tag{6}$$

If there are insufficient fringes in the transparent region, one may have to resort to using fringes from the region of weak and medium absorption, where $\alpha \sim 0$. Both extremes, T_M and T_m, are used to determine the film refractive index (n), and then M in (5) is given by

$$M = 2s\frac{T_M - T_m}{T_M T_m} + \frac{s^2 + 1}{2}. \tag{7}$$

This optical characterization method is used to determine value of the refractive index of $Se_{35}Te_{65-x}Ge_x$ films. This value is found to be 2.41 for $Se_{35}Te_{65}$ ($x = 0$), while it increases by increasing the concentration of Ge to be 2.87 at $x = 12$. The refractive index values were tabulated in Table 1. These values are comparable with those reported in similar compositions [34]. This increase in values of the refractive index of $Se_{35}Te_{65-x}Ge_x$ films might be attributed to the increased disorder in the structure [33]. Since the deposited films in this experiment have entirely amorphous structures as could be seen in the XRD results (Figure 1), further addition of impurities into the host is expected to increase disorder of the material. This might have increased values of the refractive index. Other groups have signed this

increase to the change in stoichiometry [35] and internal strain [36] of the glassy alloy with large incorporation of the impurity content.

From the application point of view, controlling the chalcogenide properties by changing the chemical composition at the nanoscale level might have great advantage for several applications. The present films of $Se_{35}Te_{65-x}Ge_x$ nanoparticles have showed interesting structural and optical properties. They remain in amorphous phase and could form uniform nanoparticles; moreover, introducing Ge into the host of this system at the nanoscale level has showed significant changes in value of the band gap and increasing values of the refractive index. These results might be useful for applications like optical recording media, xerography and electrographic applications, infrared spectroscopy, and laser fiber. Moreover, their transparency in the infrared above 800 nm and their high refractive index are good indicators for integrated optics and detection in the mid- and thermal-infrared spectral domain.

4. Conclusion

Thin films of $Se_{35}Te_{65-x}Ge_x$ ($x = 0, 3, 6, 9, 12$) nanoparticles were synthesized using thermal evaporation method. These films were found to be of amorphous nature as revealed from XRD result, while SEM images show nanoparticles with average particle sizes around 30 nm. No significant changes are observed on morphology of the deposited films by changing the concentrations of Te and Ge. The optical band gap (E_g) values were determined and are found to decrease by increasing the concentration of Ge. The absorption, extinction coefficients, and refractive index were also obtained. The transmission spectra for the thin films of $Se_{35}Te_{65-x}Ge_x$ nanoparticle show strong absorption at wavelength less than 500 nm and become highly transparent at wavelength above 800 nm. No significant changes are observed in intensity of the spectra by increasing concentration of Ge. These results might be useful for development of optical disks and other semiconducting devices based on these nanoparticle films.

Acknowledgment

The authors are thankful to the Deanship of Scientific research, King Abdulaziz University, for the financial assistance under the project no. 1431/135/28.

References

[1] H. Shi, D. Guo, and Y. Ouyang, "Structural evolution of mechanically alloyed nanocrystalline FeAl intermetallics," *Journal of Alloys and Compounds*, vol. 455, no. 1-2, pp. 207–209, 2008.

[2] M. Zakeri, M. Allahkarami, Gh. Kavei, A. Khanmohammadian, and M. R. Rahimipour, "Synthesis of nanocrystalline Bi_2Te_3 via mechanical alloying," *Journal of Materials Processing Technology*, vol. 209, no. 1, pp. 96–101, 2009.

[3] M. A. Rafea, A. A. M. Farag, and N. Roushdy, "Structural and optical characteristics of nano-sized structure of $Zn_{0.5}Cd_{0.5}S$ thin films prepared by dip-coating method," *Journal of Alloys and Compounds*, vol. 485, no. 1-2, pp. 660–666, 2009.

[4] J. Yang, G. Wang, H. Liu, J. Park, and X. Cheng, "Controlled synthesis and characterization of ZnSe nanostructures via a solvothermal approach in a mixed solution," *Materials Chemistry and Physics*, vol. 115, no. 1, pp. 204–208, 2009.

[5] K. Tripathi, A. A. Bahishti, M. A. Majeed Khan, M. Husain, and M. Zulfequar, "Optical properties of selenium–tellurium nanostructured thin film grown by thermal evaporation," *Physica B*, vol. 404, no. 16, pp. 2134–2137, 2009.

[6] M. F. Kotkata, A. E. Masoud, M. B. Mohamed, and E. A. Mahmoud, "Synthesis and structural characterization of CdS nanoparticles," *Physica E*, vol. 41, no. 8, pp. 1457–1465, 2009.

[7] N. B. Pendyala and K. S. R. K. Rao, "Temperature and capping dependence of NIR emission from PbS nano—microcrystallites with different morphologies," *Materials Chemistry and Physics*, vol. 113, no. 1, pp. 456–461, 2009.

[8] S. P. Anthony, "Synthesis of Ag_2S and Ag_2Se nanoparticles in self assembled block copolymer micelles and nano-arrays fabrication," *Materials Letters*, vol. 63, no. 9-10, pp. 773–776, 2009.

[9] A. Phuruangrat, T. Thongtem, and S. Thongtem, "Characterization of Bi_2S_3 nanorods and nano-structured flowers prepared by a hydrothermal method," *Materials Letters*, vol. 63, no. 17, pp. 1496–1498, 2009.

[10] S. Zu, Z. Wang, B. Liu, X. Fan, and G. Qian, "Synthesis of nano-$Cd_xZn_{1-x}S$ by precipitate-hydrothermal method and its photocatalytic activities," *Journal of Alloys and Compounds*, vol. 476, no. 1-2, pp. 689–692, 2009.

[11] M. Senna and S. Nakayama, "Preparation and properties of nano-amorphous organic and inorganic particles via chemical and mechanochemical routes," *Journal of Alloys and Compounds*, vol. 483, no. 1-2, pp. 265–270, 2009.

[12] M. M. El-Nahass, A. A. M. Farag, and A. A. Atta, "Influence of heat treatment and gamma-rays irradiation on the structural and optical characterizations of nano-crystalline cobalt phthalocyanine thin films," *Synthetic Metals*, vol. 159, no. 7-8, pp. 589–594, 2009.

[13] S. K. Kang, M. H. Jeon, J. Y. Park et al., "Fabrication of nanocrystalline silicon thin film at low temperature by using a neutral beam deposition method," *Journal of Crystal Growth*, vol. 312, no. 14, pp. 2145–2149, 2010.

[14] D. Gracin, J. Sancho-Paramon, K. Juraić, A. Gajović, and M. Čeh, "Analysis of amorphous-nano-crystalline multilayer structures by optical, photo-deflection and photo-current spectroscopy," *Micron*, vol. 40, no. 1, pp. 56–60, 2009.

[15] P. Sharma and S. C. Katyal, "Effect of substrate temperature on the optical parameters of thermally evaporated Ge–Se–Te thin films," *Thin Solid Films*, vol. 517, no. 13, pp. 3813–3816, 2009.

[16] M. K. R. Khan, M. A. Rahman, M. Shahjahan et al., "Effect of Al-doping on optical and electrical properties of spray pyrolytic nano-crystalline CdO thin films," *Current Applied Physics*, vol. 10, no. 3, pp. 790–796, 2010.

[17] S. Venkatachalam, Y. Kanno, and S. Velumani, "Characterization on pulsed laser deposited nanocrystalline ZnO thin films," *Vacuum*, vol. 84, no. 10, pp. 1199–1203, 2010.

[18] M. M. Larijani, M. B. Zanjanbar, and A. Majdabadi, "The effect of carbon fraction in Zr(C, N) films on the nanostructural properties and hardness," *Journal of Alloys and Compounds*, vol. 492, no. 1-2, pp. 735–738, 2010.

[19] D. H. Kuo and B. J. Chang, "Growth behaviors of ZnO nanorods grown with the Sn-based bilayer catalyst-covered substrates," *Journal of Nanomaterials*, vol. 2011, Article ID 603098, 9 pages, 2011.

[20] G. Amin, M. H. Asif, A. Zainelabdin, S. Zaman, O. Nur, and M. Willander, "Influence of pH, precursor concentration, growth time, and temperature on the morphology of ZnO nanostructures grown by the hydrothermal method," *Journal of Nanomaterials*, vol. 2011, Article ID 269692, 9 pages, 2011.

[21] Z. H. Khan, S. A. Khan, N. Salah, S. Habib, S. M. Abdallah El-Hamidy, and A. A. Al-Ghamdi, "Effect of composition on electrical and optical properties of thin films of amorphous Ga_xSe_{100-x} nanorods," *Nanoscale Research Letters*, vol. 5, no. 9, pp. 1512–1517, 2010.

[22] Z. H. Khan, S. A. Khan, S. Habib, A. A. Al-Ghamdi, and N. Salah, "Morphology and optical properties of thin films of Ga_xSe_{100-x} nanoparticles," *Nanoscience and Nanotechnology Letters*, vol. 3, pp. 319–323, 2011.

[23] Z. H. Khan, S. A. Khan, N. Salah, S. S. Habib, and A. A. Al-Ghamdi, "Electrical transport properties of thin film of a-$Se_{87}Te_{13}$ nanorods," *Journal of Experimental Nanoscience*, vol. 6, no. 4, pp. 337–348, 2011.

[24] Z. H. Khan, S. A. Khan, N. Salah, A. A. Al-Ghamdi, and S. Habib, "Electrical properties of thin films of a-Ga_xTe_{100-x} composed of nanoparticles," *Philosophical Magazine Letters*, vol. 91, no. 3, pp. 207–213, 2011.

[25] J. Tauc, in *Amorphous and Liquid Semiconductors*, J. Tauc, Ed., p. 159, Plenum Press, New York, NY, USA, 1979.

[26] F. Urbach, "The long-wavelength edge of photographic sensitivity and of the electronic absorption of solids," *Physical Review*, vol. 92, no. 5, p. 1324, 1953.

[27] M. Ilyas, M. Zulfequar, and M. Husain, "Optical investigation of a-Ga_xSe_{100-x} thin films," *Journal of Modern Optics*, vol. 47, no. 4, pp. 663–675, 2000.

[28] N. F. Mott and E. A. Davis, *Electronics Processes in Non-Crystalline Materials*, Clarendon Press, Oxford, UK, 1979.

[29] H. K. Rockstad, "Sharp absorption edges and shallow density of states tails for amorphous germanium," *AIP Conference Proceedings*, vol. 20, no. 2, pp. 18–26, 1974.

[30] T. T. Nang, M. Okuda, T. Matsushita, S. Yokota, and A. Suzuki, "Electrical and optical properties of Ge_xSe_{1-x} amorphous thin films," *Japanese Journal of Applied Physics*, vol. 15, no. 5, pp. 849–853, 1976.

[31] P. Sharma and S. C. Katyal, "Thickness dependence of optical parameters for Ge–Se–Te thin films," *Materials Letters*, vol. 61, no. 23-24, pp. 4516–4518, 2007.

[32] R. Swanepoel, "Determination of the thickness and optical constants of amorphous silicon," *Journal of Physics E*, vol. 16, no. 12, pp. 1214–1222, 1983.

[33] P. Sharma and S. C. Katyal, "Effect of tin addition on the optical parameters of thermally evaporated As–Se–Ge thin films," *Materials Chemistry and Physics*, vol. 112, no. 3, pp. 892–897, 2008.

[34] P. Sharma and S. C. Katyal, "Effect of substrate temperature on the optical parameters of thermally evaporated Ge–Se–Te thin films," *Thin Solid Films*, vol. 517, no. 13, pp. 3813–3816, 2009.

[35] K. Yamaguchi, N. Nakayama, H. Matsumoto, and S. I. Kegami, "CdS–CdTe solar cell prepared by vapor phase epitaxy," *Japanese Journal of Applied Physics*, vol. 16, no. 7, pp. 1203–1211, 1977.

[36] A. Ashour, N. El-Kadry, and S. A. Mahmoud, "On the electrical and optical properties of CdS films thermally deposited by a modified source," *Thin Solid Films*, vol. 269, no. 1-2, pp. 117–120, 1995.